Magnetically-induced synthesis of highly-crystalline ternary chalcopyrite nanocrystals under ambient conditions†

Kuan-Ting Kuo, Shang-Hsiu Hu, Dean-Mo Liu* and San-Yuan Chen*

Received 3rd September 2009, Accepted 27th November 2009
First published as an Advance Article on the web 13th January 2010
DOI: 10.1039/b918246b

We report a novel and facile method to synthesize phase pure, chemically homogeneous, and highly crystalline $CuInS_2$, an important element for optoelectronics, optics, and solar energy applications. This ternary semiconductor compound is grown by magnetic Zn doping under high-frequency magnetic induction at ambient conditions. The magnetic doping gives superparamagnetic heating of the resulting nanocrystals *via* magnetic induction, causing an accelerating growth rate of the doped $CuInS_2$ under ambient conditions of 2–3 orders of magnitude faster than conventional autoclave synthesis. Shape evolution of the Zn doped $CuInS_2$ nanocrystals from initially spherical, to pyramidal, cubic, and finally to a bar geometry, was detected as a function of time of exposure to magnetic induction. These newly-synthesized nanocrystals demonstrated considerably improved optical emission properties compared to those prepared *via* conventional autoclave methods. Nanostructural development of the nanocrystals was well characterized and a mechanism of crystal growth was proposed.

1. Introduction

The synthesis and characterization of semiconductor nanocrystals have attracted a great deal of attention due to their potential applications in the fields of magnetism, optics, electronics, optoelectronics, biomedicine, and catalysis.[1–3] These nanocrystals exhibit remarkable physical, chemical, and biological properties that can be finely tuned by adjusting the composition, size, and shape of the crystals.[4,5] A strong correlation has been demonstrated between the nanostructure of the nanocrystals and corresponding performance of the manufacturing device.[6,7] In past decades, the synthesis of group II–VI semiconductors (*i.e.*, binary semiconductor compounds) with various geometries has been successfully achieved for a number of different compositional combinations, from single phase elements to alloys and compound semiconductors.[8,9] In comparison, ternary alloys have been shown to offer more advantages over binary compounds, including continuously tunable band gaps and tailored physicochemical properties.

Colloidal semiconductors and metals have been synthesized using coordinating non-aqueous media by manipulating capping ligands, ligand-solvent pairs, reactant concentration, or synthesis temperature.[10–16] $CuInS_2$ (CIS), which is a ternary chalcopyrite compound, has demonstrated more optically and electronically tunable properties than the binary II–VI analogues with the cubic zinc blende structure. CIS has recently been considered to be a promising candidate for photovoltaic applications, owing to its relatively high absorption coefficient and excellent energy matching between its band gap (1.5 eV) and the solar spectrum. CIS nanocrystals have been synthesized by processes such as the elemental solvothermal technique,[17–19] thermolysis,[20,21] the hot injection technique,[22,23] and the single-source precursor route.[24,25] All of these techniques require high temperature and/or high pressure environments in order to bring the various kinds of species into the desirable crystal form. However, compared with the significant progress in monodisperse binary chalcopyrite colloids, investigation of ternary chalcopyrite colloids has been limited, owing to the lack of suitable synthesis methods. Therefore, the challenge remains in the preparation of monodisperse ternary chalcopyrite colloids with manageable size and shape.

Making ternary chalcopyrite compounds with superparamagnetic behavior by magnetic doping has not yet been tried. It is generally understood that incorporation of magnetic elements might enable the host materials to exhibit magnetic behavior.[26–29] By limiting the size of the resulting doped compound to a few nanometres in scale, superparamagnetic character may be developed. Room-temperature ferromagnetism has been reported for non-magnetic metallic (Pd and Au) nanoparticles and carbon nanostructures (nanographites and polymerized fullerenes).[30–34] The ternary chalcopyrite semiconductors, expressed as I–III–VI2, are considered to be a superstructure of the zinc blende type. In particular, $CuAB_2$ (A = Al, Ga, In; B = S, Se) has shown intrinsic p-type conductivity, which suggests that chalcopyrite compounds might be interesting host materials for magnetic doping. CIS nanocrystals have been found to exhibit magnetic properties in a limited number of reports.[35,36a] Taking these findings into consideration, we hypothesized that a new synthesis technology could be advanced by magnetic doping, in which CIS nanocrystal nucleation

Department of Materials Sciences and Engineering, National Chiao Tung University, 1001 Ta-Hsueh Rd., 300 Hsinchu, Taiwan, ROC. E-mail: u9318833.mse93g@nctu.edu.tw; sshow210@yahoo.com.tw; deanmo_liu@yahoo.ca; sanyuanchen@mail.nctu.edu.tw; Fax: +886-3-5725490; Tel: +886-3-5731818

† Electronic supplementary information (ESI) available: absorption and photoluminescence spectra; EDX spectra and TEM image; XRD pattern; magnetization curves; mechanism of 'first paramagnetic nanocrystal' formation; HRTEM images; duration times of precursor; zeta-potential values. See DOI: 10.1039/b918246b

and growth could be self-manipulated *via* magnetically induced heating of the developing CIS nanocrystals upon synthesis. This is in contrast to the currently existing time-consuming, cost-ineffective, and eco-unfriendly autoclaving synthesis.

Here, we report a novel methodology in the synthesis of CIS nanocrystals in coordinating solvents without sequential chalcogenide precursor injection, which is achieved by incorporation of magnetic Zn species, *i.e.*, diethyldithiocarbamide zinc (DECZn), following a high frequency magnetic field (HFMF) induction (Fig. 1) under ambient conditions. The process for growing the resulting Zn-doped CIS nanocrystals with definite geometrical evolution can then be developed and controlled.

2. Experimental

2.1 Chemicals

Copper(I) chloride (CuCl, 95%, analytical reagent), indium(III) chloride ($InCl_3$, 98%, AR), and trioctylphosphine (TOP, 90%, technical grade) were purchased from Sigma-Aldrich Corp.; octadecene (ODE, 90%, technical grade), oleylamine (70%, technical grade), and diethyldithiocarbamic acid zinc salt ($[(C_2H_5)_2NCSS]_2Zn$, technical grade) were purchased from Tokyo chemical industry Co., Ltd.

2.2 Synthesis of Zn-CIS nanocrystals

0.5 mmol diethyldithiocarbamic acid zinc salt was dissolved in 6 ml TOP. The solution was diluted with 24 ml ODE to form a clear solution (solution 1). Then, 0.2 mmol CuCl and $InCl_3$ were dissolved in 6 ml oleylamine at 50 °C to form another solution (solution 2). Here, amine coordinates the Cu and In ions to produce amine complexes. These two solutions were mixed to produce the raw material solution. A small aliquot of raw material solution was put into a test tube and exposed to HFMF with an input power of 90 W (Fig. 1). The color of the mixture solution was changed with different durations of HFMF exposure from yellow (30 s), red (45 s) to black (120 s). The resulting precipitated powders were collected *via* centrifugation at 6000 rpm, removed from the solution, and repeated three times to remove excess surfactants which were precipitated using methanol. A high frequency (50–100 kHz) magnetic field (HFMF) was applied to the precursors to provide kinetic energy for Zn-CIS nanocrystal synthesis. The HFMF was created by a power supply, function generator, amplifier, and cooling water.

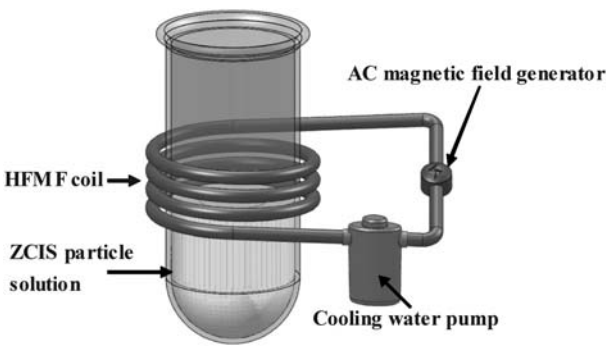

Fig. 1 Apparatus setup for the magnetically-induced synthesis.

Similar equipment was also reported previously.[36b] The strength of the magnetic field depended on the coils.

2.3 Characterization

In this study, the coil was 8 loops, the frequency was 50 kHz and the strength of magnetic field (H) was 2.5 kA m^{-1}. The temperature of the HFMF generator was controlled by cycling cooling water at 25 °C. The resulting powder collected from the solutions was examined using X-ray powder diffraction (XRD, M18XHF, Mac Science, Japan) to identify the crystallographic phase of nanocrystals, with Cu-Kα radiation (λ = 0.15405 nm) (40 kV, 200 mA), 2θ ranging from 10° to 70° at a scanning rate of 10° min^{-1}. The morphological structure of the Zn-CIS nanocrystals was examined using a JEOL 2100 transmission electron microscope (TEM) operating at 200 kV. A UV-vis spectrophotometer (UV-1600; Agilent 8453) and PL emission spectrofluorometer (FP-6600; Jasco, Inc., Japan) were used to characterize the optical properties of the resulting Zn-CIS nanocrystals. Measurements of magnetization (M) *versus* applied field H and temperature T were carried out using a commercial SQUID (superconducting quantum interference device) magnetometer (MPMX-XL7).

3. Results

3.1 Optical behavior

A solution mixture of copper chloride (CuCl) and indium chloride ($InCl_3$) precursors was first prepared by dissolving in oleylamine and diluted with octadecene, followed by a trioctylphosphine (TOP) capping agent. Judicious choice of the precursor ratio results in nanocrystals with a tunable [Zn]/[Cu] composition. The mixed solution was subjected to HFMF for crystal growth. The size and shape of the resulting nanoparticles could be finely tuned by varying the exposure time and concentration of the capping agent during the synthesis. Under 90 W AC magnetic induction, the appearance of the solution underwent a sharp change in color from yellow to red, over a time period of 45 s, and then turned to black after two minutes of induction. However, without the addition of Zn precursor, the solution mixture showed no change in appearance even for a long duration of magnetic induction. To investigate the effect of magnetic induction, aliquots of the Zn-doped solutions with different time durations from 30 to 360 s were taken and examined by ultraviolet-visible spectroscopy, photoluminescence spectroscopy, and transmission electron microscopy. The fluorescent Zn-doped $CuInS_2$ nanocrystals started to appear in the solution within the first 60 s and while under 365 nm UV light exposure, the solutions showed a yellow (30 s) and red (45 s) appearance (Fig. S1, ESI†). These two samples with emission peaks at 590 and 630 nm were similar to those reported by Nakamura *et al.*,[37] who observed an improved PL intensity when Zn was incorporated into CIS nanocrystals, due to a reduction of anti-site defects.[38] The UV-vis spectra of these samples (30, 45, 180, 300, and 420 s, respectively) show the typical absorption curve of a semiconductor material (Fig. 2): a band-edge peak was visible at around 390 and 800 nm. The absorption energies for a 180 s exposure were significantly shifted to that of bulk $CuInS_2$ (*ca.* 810 nm), consistent with the expected effects of quantum

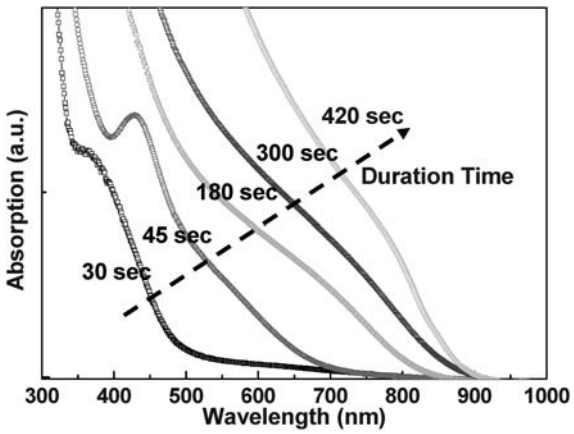

Fig. 2 UV-vis absorption spectra of Zn-CIS nanocrystals under magnetic exposure (from left to right: 30, 45, 180, 300, and 420 s).

confinement. More evidence for the size confinement effect was provided by PL spectroscopy (Fig. S1, ESI†). The PL spectrum of the Zn-CIS colloids showed a blue shift compared to those in bulk CIS, which suggests further the size-dependent optical properties of the colloids. However, after long-term magnetic exposure, the absorption spectrum shifts to a longer wavelength, and a broad shoulder develops at 800 nm. The shift of the absorption spectrum to a longer wavelength with increasing photolysis time is consistent with band gap narrowing due to particle growth. The absorbance range broadens from 390 to 800 nm (corresponding to particle size increasing from 3.5 to 75.4 nm), indicating the band gap of the Zn-CIS nanocrystals underwent a red shift to match the bulk CIS (1.5 eV, 810 nm).

3.2 Growth of Zn-CIS nanocrystals

The TEM image of these Zn-doped nanocrystals showed narrowly size-distributed nanoparticles, with an average diameter of 3.5 nm (Fig. 4(a)). The high-resolution TEM image (Fig. 3(a)) further indicated that these nanoparticles were single crystalline and spherical in shape. The size-specific quantum confinement of this size of Zn-CIS nanocrystals gave a red solution. However, after only two minutes of magnetic field exposure, these nanocrystals grew to a size larger than the Wannier–Mott bulk exciton radius (*i.e.*, 8.1 nm for CIS[39]). To identify the crystal growth of the Zn doped chalcopyrite semiconductor under magnetic exposure, solution samples were taken after magnetic induction for durations of 180, 300, and 420 s, where a steady-state development of the resulting nanocrystals is assumed, albeit unintentionally selected. For the 180 s duration, the colloidal Zn-CIS nanocrystals displayed a rectangular geometry, with a size of 12–15 nm in length (Fig. 3(b)). In the TEM images, lattice fringes corresponding to {0−11} and {220} CIS planes were predominantly visible. Based on these observations, the structure of the Zn-CIS nanocrystals after 180 s of magnetic induction was confirmed to be trigonal-pyramidal, rather than trigonal-plate, and has been formulated for $CuInSe_2$[40] and CdS.[41] After 300 s of induction, a nanocubic geometry was obtained (from the same batch of solution), as shown in Fig. 3(c).

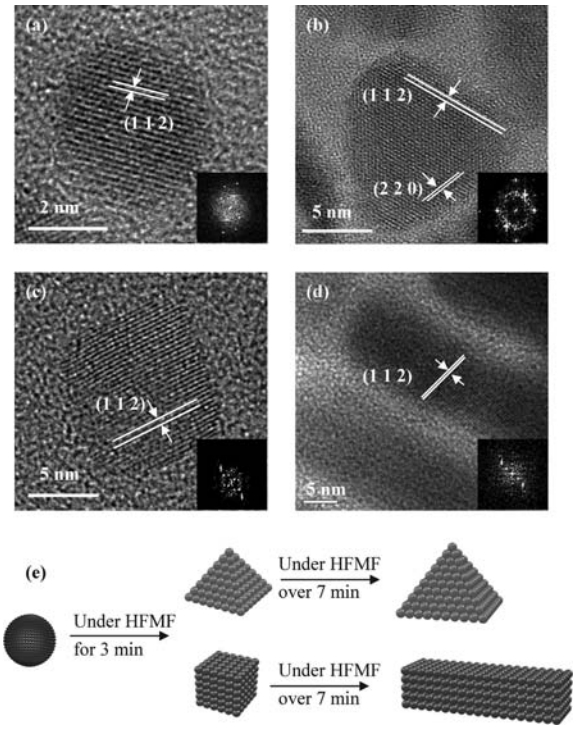

Fig. 3 HRTEM images of the Zn-CIS nanocrystals with various geometries: (a) nanoparticles, (b) nanopyramids, (c) nanocubes, (d) nanobars synthesized under magnetic exposure. (e) Schematic of the growth of nanoparticles into various geometries of different sizes, from nanopyramids, nanocubes, and nanobars under magnetic induction.

The lattice fringes are separated by a distance of 3.1 Å, which corresponds to the {112} planes of CIS. The surface tension values of the {100}, {010}, and {001} planes of nanocubes are

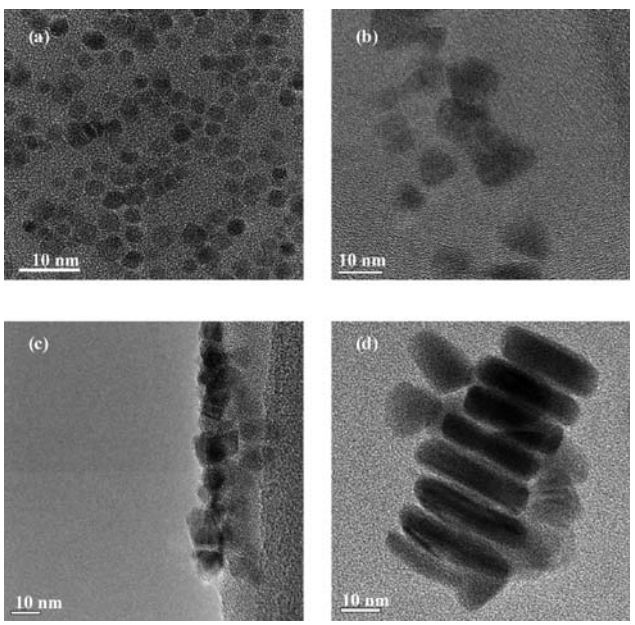

Fig. 4 TEM images of samples: (a) nanoparticles, (b) nanopyramids, (c) nanocubes, (d) nanobars. All the images have the same scale bars (10 nm).

very similar, resulting in a similar distance between these three crystallographic faces and the Wulff's point. On this basis, a higher average growth rate along those crystallographic directions is expected, resulting in Zn-CIS nanocrystals evolving into rectangular or quasi-cubic geometry. Nevertheless, after 420 s of magnetic induction, the {112} plane of the nanocube showed the fastest growth rate to form a bar-like geometry with an average length of 75.4 nm and width of 18.3 nm (Fig. 3(d)).

Lower-magnification TEM investigations were performed to monitor the formation of Zn-CIS nanocrystals. As shown in Fig. 4(a), spherical particles dominantly appeared in the solution in the 60 second sample. After 180 s, most of the spherical structures were replaced by nanopyramids with diameters of 12–15 nm, as shown in Fig. 4(b), indicating that the nanoparticles were transformed in the magnetic field. The nanocubes (Fig. 4(c)) were formed after 300 s and then eventually grew into nanobars after 420 s, Fig. 4(d). It appears from experimental observations that both the pyramidal and cubic Zn-CIS nanoparticles co-existed in the time duration of 300–420 s (Fig. S2, ESI†). The nanocubes kept growing along the (112) plane and turned into a nanorod geometry; in the meantime, the small pyramidal nanoparticles kept growing equally along the four faces and turned into large crystals of identical geometry (see Fig. 3(e) for a better illustration). In other words, both the nanorod and nanopyramid Zn-CIS crystals of larger dimensions, after a longer magnetic exposure, were present simultaneously in the final suspension. However, it is not fully understood whether any interactions evolved between the growth of both types of nanocrystals.

In a chalcopyrite $CuInS_2$ crystal, the bonding energy between Cu and S atoms is weaker than that between In and S atoms, which means that the Cu vacancy is preferably generated. In addition, the Cu vacancies induce anti-site defect generation.[38] Furthermore, the ionic diameter of Cu (0.635 A) is similar to that of Zn (0.64 A). On this basis, the Cu site in the lattice is preferentially substituted by Zn where such a substitution is found to be more energetically favorable to prevent anti-site defects.[38] The molar ratios of Zn : Cu : In : S in the nanocrystals of varying stages of magnetic induction were determined by inductively couple plasma (ICP) spectroscopy and TEM-EDX analysis (Fig. S2, ESI†): both sets of data showed consistent ratios with an average of 1.1 : 2.5 : 3.4 : 5.6, *i.e.*, a Cu-rich phase, for various geometrical structures, as given in Table 1. These results indicated that a relatively uniform compositional evolution of these Zn-CIS nanocrystals can be achieved.

3.3 Crystallographic analysis

The crystal phase of the as-synthesized compound was identified by powder X-ray diffraction (XRD) (Fig. 5, black vertical lines

Table 1 Composition of the varied structure Zn-CIS nanocrystal

	Zn (%)	Cu (%)	In (%)	S (%)	Ratio
Nanoparticle	8.73	19.84	26.98	44.44	1.1 : 2.5 : 3.4 : 5.6
Pyramid	8.46	19.6	28.07	43.87	1.1 : 2.5 : 3.6 : 5.7
Cube	9.01	19.67	27.45	44.87	1.1 : 2.4 : 3.4 : 5.5
Bar	9.34	19.42	27.75	43.49	1.2 : 2.5 : 3.6 : 5.6

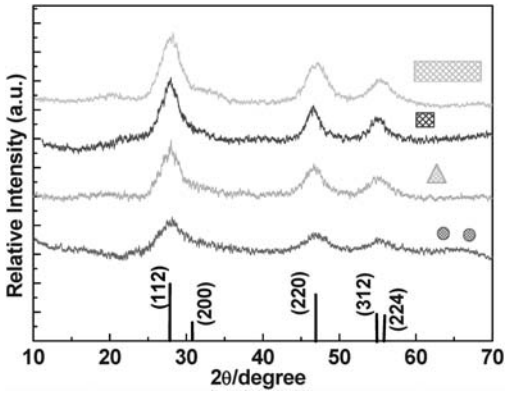

Fig. 5 XRD patterns of the Zn-CIS nanocrystals of different shapes, with vertical lines on the *x*-axis denoting the standard CIS powder diffraction pattern.

on the *x*-axis denote the $CuInZnS_2$ diffraction pattern, JCPDS No. 47-1731) and higher energy XRD (Fig. S3, ESI†), which clearly reveals that all the diffraction peaks perfectly match the crystallographic structure of chalcopyrite $CuInZnS_2$ (space group: $I42d$ (No. 122) and unit cell dimensions: $a = b = 5.508$ Å, $c = 11.09$ Å), with no other impurity phases detected, indicating that a phase-pure Zn doped CIS can be efficiently obtained. Moreover, regardless of the particle size (ranging from 3.5 to 75.4 nm) of the synthesized Zn-CIS nanocrystals, they all gave identical diffraction patterns. These results, together with the HR-TEM observations, further prove that all the Zn-CIS nanocrystals synthesized under magnetic induction possess single-crystal structure with a relatively high degree of uniformity. Although the variation of crystal shape has been addressed in a number of articles, the details of the mechanism have not yet been clarified.[42–45] It is generally believed that the shape evolution of the nanocrystals is dominated by the inherent crystal structure during the initial nucleation stage. The subsequent growth was then managed through the delicate control of external factors, such as surfactants, temperature, and time.[46]

4. Discussion

The discovery of magnetic-induced synthesis of a ternary semiconductor is far beyond what has been observed to date using traditional solution chemistry, such as the solvothermal method, where temperatures as high as 200–300 °C over time periods of several to dozens of hours are frequently required. The magnetic-induced crystal growth of Zn-doped CIS in this investigation should cause a self-heating effect originating from the developing Zn-CIS compound, since the CIS nanocrystals showed a stronger paramagnetic behavior after doping with Zn, Fig. 6. The hysteresis loop for the resulting Zn-CIS nanocrystals was corrected for the diamagnetic contribution (inset of Fig. 6) and shows typical paramagnetic behavior, with the magnetization essentially saturated above 10 kOe. The hysteresis loop data for the Zn-CIS nanocrystals at 300 K and 5 K (Fig. S4, ESI†) also evidenced the superparamagnetism of such Zn-doped CIS nanocrystals. In theory, magnetic colloids in a magnetic field experience an internal stress as a result of the non-uniform distortion arising from magnetic forces, generating heat. Under

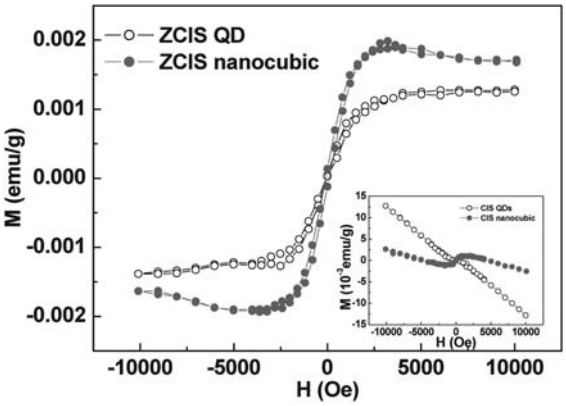

Fig. 6 Magnetization curves measured at room temperature for Zn-CIS QDs (open symbols) and Zn-CIS nanocubes (filled symbols). The inset shows the raw data and the data after subtracting the high-field diamagnetic component.

magnetic induction, the temperature of the Zn-CIS colloidal solution gradually rose from the very beginning and reached a steady-state temperature of several tens of Celsius, at which point the heat generation from the magnetic Zn-CIS nanocrystals was equilibrated with the heat dissipated to the environment.

Assuming magnetic heating involves only isolated, independent nanoparticles, RF field friction in and around a magnetic particle can stem from two sources.[47] First, the particle may tumble causing frictional heating at the particle–solvent interface. The relaxation time for this mode can be estimated as the time required for Brownian motion over a characteristic distance of the order of one particle diameter. Brownian relaxation may not be responsible for the frictional heating of the Zn-CIS, however, because the heat generated from this mechanism should be equally shared between the nanoparticle and solvent so it is unlikely for the Zn-CIS alone to reach a very high temperature. Friction may also arise from spin rotation without crystal lattice rotation within the crystal. The relaxation time for this mode (Neel relaxation) is the reciprocal of the spin flipping rate, too fast to contribute any significant friction in a RF field. As a first approximation, we can roughly approximate the heating rate R_{ZCIS} of the Zn-CIS (or ZCIS) nanoparticles in terms of R_S using $V_{ZCIS}R_{ZCIS}C_{ZCIS} = (1 - V_{ZCIS})R_SC_S$. Here V_{ZCIS} is the volume fraction of the Zn-CIS nanocrystals relative to the solution, and C_S and C_{ZCIS} are the volumetric specific heats of the solvent and ZCIS, respectively. Here we used $V_{ZCIS} \sim 0.01$, meanwhile, referring to the specific heat of ZCIS and the solvent, we estimate $C_S/C_{ZCIS} \sim 1$. Therefore, the calculated R_{ZCIS} is from 10 °C s^{-1} to 100 °C s^{-1}, *i.e.*, it takes a few to a few tens of seconds for the temperature to rise to several hundred degrees Celsius in the Zn-CIS nanocrystals before a steady state is reached. However, interfacial heat transfer at a nanometre scale surrounding the nanocrystals is not well determined.

Referring back to the formation of such Zn-CIS nanocrystals under magnetic field, how do these particles form in the first place? In the solution without adding Zn precursor (which is virtually a Zn–S-containing precursor), the other two precursors (*i.e.*, Cu and In) are unable to react in the presence of the magnetic field (we have also found no reaction with Zn–S-containing precursor alone). However, after the Zn–S-containing precursor was prepared separately, *i.e.*, completely dissolved in a solvent, we found no precipitate in the solution and believe it may form a Zn–S-containing compound. While the first aliquot amount of the compound was added to the mixture solution, energetically effective collisions (under heating and agitating) among those precursors should cause the incorporation of Cu ion with the compound (due to the similar ionic size between Cu and Zn ions), upon which a chemically equivalent mixture of the those molecular precursors may develop into the first nanocrystal or "to the field. Since the electron configuration of Cu^+ is d^{10}, ZnS doped with Cu^+ would be diamagnetic. If copper existed as Cu^0 or Cu^{2+} in ZnS, the system would be strongly paramagnetic.[48] In our study, the Cu precursor is CuCl, which means Cu^+ could be pseudo-oxidized by the Zn–S-containing compound (*i.e.*, S^- in the Zn precursor, Scheme S1 in ESI†). While the Cu-containing ZnS compound exhibits paramagnetism, the magnetic field can thus induce heat. To prove our hypothesis for the formation of a chemical compound, we mixed only the Cu precursor into the solution of Zn–S-containing precursor, in the absence of In precursor. A secondary force may cause interaction between Cu and S ions, rather than forming any chemical bond, leading to a featureless Cu–S bond using Raman spectroscopic analysis; in other words, there appears no chemical interaction between Cu and S in the mixture. In spite of such weak attraction, the reaction is somehow an ongoing procedure in the presence of the magnetic field which was confirmed by a visual observation of the solution, which changed from turbid to transparent. This phenomenon indicated the precursors in the solution were actually affected by the magnetic field and consequently induced heating for further reaction. Although we have no direct evidence available for such an intermediate compound presently, the SQUID analysis of collected precipitate from the mixed Zn–S and Cu precursors demonstrated our hypothesis (see Fig. S5, ESI†). It is highly likely that the "first" magnetic nanocrystal may remain for a short period of time and form rapidly into a more stable nanocrystal with Zn–Cu–In–S near-stoichiometric chemistry under the presence of magnetic field due to the involvement of other ions, such as In. Once the first paramagnetic Zn-CIS nanocrystal was developed, a continuous growth followed immediately and rapidly. Development of such a "first paramagnetic nanocrystal" in the solution should be time dependent, following a crystal growth kinetic, both scenarios result in a mixture of nanocrystals of varying geometry and size over a certain time span of reaction, as evidenced in Fig. 3, where nanocrystals with different sizes and shapes can be observed simultaneously.

Accordingly, the formation of Zn-CIS nanocrystals arising from magnetic induction is associated with fast nucleation and growth kinetics. In other words, once the nuclei begin evolving, a rapid temperature rise in the Zn-CIS nuclei should promote fast atomic deposition from the surrounding precursor bath. The exchange of heat and mass between the growing hot nanocrystals and the surrounding cold solvent due to convection should accelerate the atomic deposition of the precursors. One important feature of this synthesis is that the hot nanocrystals are likely to impart energy to the impacting precursor molecules which carry an organic part, where a further thermal dissociation of the

organic compartment at the points of deposition or collision should take place upon numerous collisions between the precursor molecules and growing nanocrystals. This results in a chemically pure deposition, leaving behind the organic counterparts in the solvent medium, as is further evidenced in the HR-TEM images (Fig. 3), where highly orderly-arranged texture of the Zn-CIS lattice for the nanocrystals from smallest to largest dimensions can be resolved at various time periods of synthesis. This result is not possible for solvothermal or similar techniques, except at relatively high temperatures, *e.g.*, >200 °C, for a long synthesis duration, *e.g.*, >10 h, where the resulting ternary nanocrystals showed very poor crystallinity (Fig. S6, ESI†) and poor optical behavior. Incorporation of organic molecules into the developing semiconductor nanocrystals may be one critical factor deteriorating the desired properties.

It is also surprisingly to learn that a highly uniform compositional development of nanocrystals of various geometries can be achieved, which suggests that the co-deposition of all those molecular precursors over the time span of the synthesis is kinetically similar. In other words, once the nanocrystals were initially evolved, the potential of those precursors upon impingement to the growing nanocrystals should be energetically similar. Such a collision should be a matter of an interaction between the precursor and nanocrystals, as a result of interparticle attraction. This is further evidenced with a subsequent zeta potential measurement (ESI† Table 2) of the nanocrystals. The zeta potential value of Zn-CIS nanocrystals was slightly negative with an average value of -10.8 ± 3.2 mV for various geometrical structures. These slightly negatively charged nanocrystals should exert weak attraction to the precursors, following a kinetically similar impingement to form the final Zn-CIS crystals. However, the Cu-rich phase evolution of the nanocrystals suggests that when incorporated into the lattice the Cu precursor tends to form a lowest-energy solid solution compared to those with the Zn precursor. Furthermore, the maximum amount of Cu substitution by Zn in the development of the energetically stable Zn-CIS nanocrystals in this finding is approximately 32.43%.

In order to distinguish the difference between magnetically-induced synthesis and the high-temperature organic solvent method (HTOSM), we compared our nanocrystal with the one reported by Nakamura *et al.*[37] The optical properties, including PL and UV-vis characteristics, are presented in Fig. 7. There are two emission peaks located at 420 and 560 nm of the HTOSM sample. The 420 nm peak contributed from the ZnS indicates an insufficient energy transition in HTOSM to permit alloying of the Zn atom into the CIS lattice and form a secondary phase, ZnS. This result confirmed our hypothesis of energy transfer through magnetic induction. Moreover, the UV-vis absorption spectrum of the Zn-CIS nanocrystals prepared with magnetic induction shows a stronger and sharper peak compared to the Zn-CIS nanocrystals prepared through HTOSM. The relatively sharp exciton peak in the absorbance spectra indicates that the Zn-CIS nanocrystals are relatively size- and shape-monodisperse. Furthermore, the optical properties are much better with band edge PL and narrow peak widths compared with the nanocrystals prepared from HTOSM.

While some studies have reported decent results of CIS[49–53] and CISe[53,54] ($CuInSe_2$) nanocrystals recently, few of them exhibited quantum-confinement behavior. Nevertheless, all of these reports need rigorous conditions such as high temperature (180–300 °C), long crystal-growth duration (1–24 h), and non-oxygen environment. Compared to those experiment conditions, magnetically-induced Zn-CIS synthesis is much more easy and fast for such nanocrystal development. This distinct feature further confirms the promising development of magnetically-induced Zn-CIS synthesis over conventional high-temperature pathways.

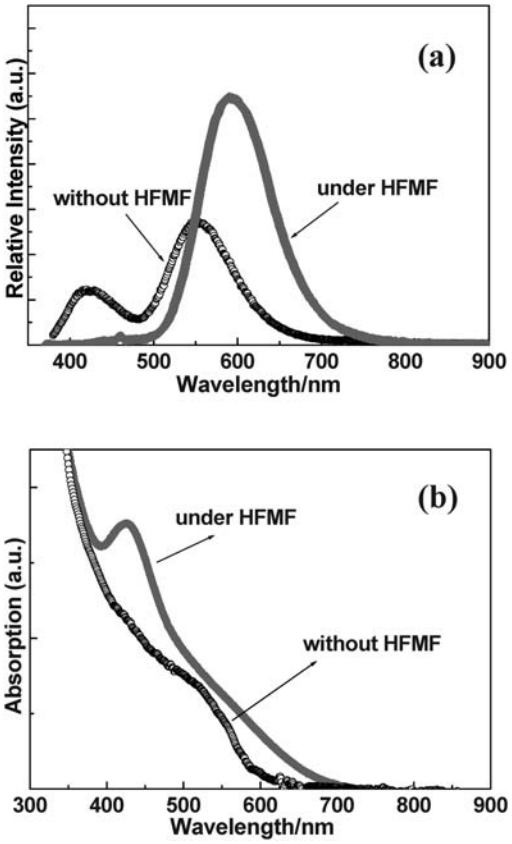

Fig. 7 Fluorescence (a) and absorption (b) spectra of the Zn-CIS nanocrystals obtained with and without magnetic induction. The excitation wavelength for the fluorescence measurements was 366 nm.

5. Conclusion and implications

A novel method using magnetic doping to form highly-crystalline semiconductor compounds in an ambient environment has been explored for the first time. The geometries and lengths of the resulting Zn-doped CIS nanocrystals can be manipulated as a function of the duration in a high-frequency magnetic field. The Zn-CIS nanocrystals exhibited excellent phase pure optical properties and chemically pure crystallinity compared to those prepared *via* conventional high-temperature methods. The UV-vis absorption spectrum of the Zn-CIS colloids has a strong absorption over a relatively wide region from UV to near IR, depending on the dimensional evolution of the Zn-CIS nanocrystals, indicating that the highly-crystalline Zn-CIS colloidal compound prepared in this work can be considered as a potential candidate for solar absorption. Such a magnetically-induced synthesis technology offers great advantages over currently

existing methodologies for the growth of these nanocrystals, resulting in better crystalline development and compositional uniformity for such a complex semiconductor compound. Such a novel synthesis method provides a new avenue for the development of ternary chalcopyrite materials *via* magnetic doping. We also believe that an expansion of such a synthesis technique can be adapted to other important semiconductor compounds, resulting in considerable improvement in purity and optically tunable properties.

Notes and references

1 A. N. Shipway, E. Katz and I. Willner, *ChemPhysChem*, 2000, **1**, 18–52.
2 S. Link and M. A. El-Sayed, *Annu. Rev. Phys. Chem.*, 2003, **54**, 331–366.
3 M. Green, *Chem. Commun.*, 2005, 3002–3011.
4 Y. Yin and A. P. Alivisatos, *Nature*, 2005, **437**, 664–670.
5 L. R. Hirsch, A. M. Gobin, A. R. Lowery, F. Tam, R. A. Drezek, N. J. Halas and J. L. West, *Ann. Biomed. Eng.*, 2006, **34**, 15–22.
6 M. H. Zhao, Z. L. Wang and S. X. Mao, *Nano Lett.*, 2004, **4**, 587–590.
7 R. Narayanan and M. A. El-Sayed, *Nano Lett.*, 2004, **4**, 1343–1348.
8 S. Sun, C. B. Murray, D. Weller, L. Folks and A. Moser, *Science*, 2000, **287**, 1989–1992.
9 S. Chen, Z. L. Wang, J. Ballato, S. H. Foulger and D. L. Carroll, *J. Am. Chem. Soc.*, 2003, **125**, 16186–16187.
10 X. Peng, U. Manna, W. Yang, J. Wickham, E. Scher, A. Kadavanich and A. P. Alivisatos, *Nature*, 2000, **404**, 59–61.
11 V. F. Puntes, D. Zanchet, C. K. Erdonmez and A. P. Alivisatos, *J. Am. Chem. Soc.*, 2002, **124**, 12874–12880.
12 N. Cordente, C. Amiens, B. Chaudret, M. Respaud, F. Senocq and M. J. Casanove, *J. Appl. Phys.*, 2003, **94**, 6358–6365.
13 C. Qian, F. Kim, L. Ma, F. Tsui, P. Yang and J. Liu, *J. Am. Chem. Soc.*, 2004, **126**, 1195–1198.
14 D. V. Talapin, R. Koeppe, S. Goetzinger, A. Kornowski, J. M. Lupton, A. L. Rogach, O. Benson, J. Feldmann and H. Weller, *Nano Lett.*, 2003, **3**, 1677–1681.
15 M. Yin, Y. Gu, I. L. Kuskovsky, T. Andelman, Y. Zhu, G. F. Neumark and S. O'Brien, *J. Am. Chem. Soc.*, 2004, **126**, 6206–6207.
16 D. J. Milliron, S. M. Hughes, Y. Cui, L. Manna, J. Li, L. –W. Wang and A. P. Alivisatos, *Nature*, 2004, **430**, 190–195.
17 J. Xiao, Y. Xie, Y. Xiong, R. Tang and Y. T. Qian, *J. Mater. Chem.*, 2001, **11**, 1417–1420.
18 B. Li, Y. Xie, J. Huang and Y. T. Qian, *Adv. Mater.*, 1999, **11**, 1456–1459.
19 Y. Jiang, Y. Wu, X. Mo, W. C. Yu, Y. Xie and Y. T. Qian, *Inorg. Chem.*, 2000, **39**, 2964–2965.
20 S. L. Castro, S. G. Bailey, R. P. Raffaelle, K. K. Banger and A. F. Hepp, *J. Phys. Chem. B*, 2004, **108**, 12429–12435.
21 S. L. Castro, S. G. Bailey, R. P. Raffaelle, K. K. Banger and A. F. Hepp, *Chem. Mater.*, 2003, **15**, 3142–3147.
22 M. A. Malik and P. O'Brien, *Adv. Mater.*, 1999, **11**, 1441–1444.
23 H. Z. Zhong, Y. C. Li, M. F. Ye, Z. Z. Zhu, Y. Zhou, C. H. Yang and Y. F. Li, *Nanotechnology*, 2007, **18**, 025602.
24 L. Tian, H. I. Elim, W. Ji and J. J. Vittal, *Chem. Commun.*, 2006, 4276–4278.
25 K. K. Banger, M. H. C. Jin, J. D. Harris, P. E. Fanwick and A. F. Hepp, *Inorg. Chem.*, 2003, **42**, 7713–7715.
26 T. Kamatani and H. Akai, *Mater. Sci. Semicond. Process.*, 2003, **6**, 389–391.
27 L. –H. Ye, A. J. Freeman and B. Delley, *Phys. Rev. B: Condens. Matter Mater. Phys.*, 2006, **73**, 033203.
28 K. R. Kittilstved and D. R. Gamelin, *J. Am. Chem. Soc.*, 2005, **127**, 5292–5293.
29 G. Z. Xing, J. B. Yi, J. G. Tao, T. Liu, L. M. Wong, Z. Zhang, G. P. Li, S. J. Wang, J. Ding, T. C. Sum, C. H. A. Huan and T. Wu, *Adv. Mater.*, 2008, **20**, 3521–3527.
30 T. Shinohara, T. Sato and T. Taniyama, *Phys. Rev. Lett.*, 2003, **91**, 197201.
31 B. Sampedro, P. Crespo, A. Hernando, R. Litran, J. C. Sanchez Lopez, C. Lopez Cartes, A. Fernandez, J. Ramirez, J. Gonzalez Calbet and M. Vallet, *Phys. Rev. Lett.*, 2003, **91**, 237203.
32 P. Crespo, R. Litran, T. C. Rojas, M. Multigner, J. M. de la Fuente, J. C. Sanchez Lopez, M. A. Garcia, A. Hernando, S. Penades and A. Fernandez, *Phys. Rev. Lett.*, 2004, **93**, 087204.
33 Y. Yamamoto, T. Miura, M. Suzuki, N. Kawamura, H. Miyagawa, T. Nakamura, K. Kobayashi, T. Teranishi and H. Hori, *Phys. Rev. Lett.*, 2004, **93**, 116801.
34 T. L. Makarova, B. Sundqvist, R. Hohne, P. Esquinazi, Y. Kopelevich, P. Scharff, V. A. Davydov, L. S. Kashevarova and A. V. Rakhmanina, *Nature*, 2001, **413**, 716–718.
35 N. Tsujii, H. Kitazawa and G. Kido, *Phys. Status Solidi A*, 2002, **189**, 951–954.
36 (*a*) A. Pietnoczka, R. Bacewicz and S. Schorr, *Phys. Status Solidi A*, 2006, **203**, 2746–2750; (*b*) R. Mohr, K. Kratz, T. Weigel, M. Lucka-Gabor, M. Moneke and A. Lendlein, *Proc. Natl. Acad. Sci. U. S. A.*, 2006, **103**, 3540–3545.
37 H. Nakamura, W. Kato, M. Uehara, K. Nose, T. Omata, S. O.-Y. Matsuo, M. Miyazaki and H. Maeda, *Chem. Mater.*, 2006, **18**, 3330–3335.
38 T. Yamamoto, I. V. Luck, R. Scheer and H. Katayama-Yoshida, *Phys. B*, 1999, **273–274**, 927–929.
39 C. Czekelius, M. Hilgendorff, L. Spanhel, I. Bedja, M. Lerch, G. Muller, U. Bloeck, D. Su and M. Giersig, *Adv. Mater.*, 1999, **11**, 643–646.
40 B. Koo, R. N. Patel and B. A. Korgel, *J. Am. Chem. Soc.*, 2009, **131**, 3134–3135.
41 N. Pinna, K. Weiss, J. Urban and M. P. Pileni, *Adv. Mater.*, 2001, **13**, 261–264.
42 Y. Cui, J. Ren, G. Chen, Y. Qian and Y. Xie, *Chem. Lett.*, 2001, 236–237.
43 W. Han, L. Yi, N. Zhao, A. Tang, M. Gao and Z. Tang, *J. Am. Chem. Soc.*, 2008, **130**, 13152–13161.
44 S. –H. Choi, E. –G. Kim and T. Hyeon, *J. Am. Chem. Soc.*, 2006, **128**, 2520–2521.
45 D. Pan, L. An, Z. Sun, W. Hou, Y. Yang, Z. Yang and Y. Lu, *J. Am. Chem. Soc.*, 2008, **130**, 5620–5621.
46 S. M. Lee, S. N. Cho and J. W. Cheon, *Adv. Mater.*, 2003, **15**, 441–444.
47 R. E. Rosensweig, *J. Magn. Magn. Mater.*, 2002, **252**, 370–374.
48 C. Corrado, Y. Jiang, F. Oba, M. Kozina, F. Bridges and J. Z. Zhang, *J. Phys. Chem. C*, 2009, **113**, 3830–3839.
49 S. T. Connor, C. –M. Hsu, B. D. Weil, S. Aloni and Y. Cui, *J. Am. Chem. Soc.*, 2009, **131**, 4962–4966.
50 R. Xie, M. Rutherford and X. Peng, *J. Am. Chem. Soc.*, 2009, **131**, 5691–5697.
51 Y. Qi, Q. Liu, K. Tang, Z. Liang, Z. Ren and X. Liu, *J. Phys. Chem. C*, 2009, **113**, 3939–3944.
52 H. Zhong, Y. Zhou, M. Ye, Y. He, J. Ye, C. He, C. Yang and Y. Li, *Chem. Mater.*, 2008, **20**, 6434–6443.
53 M. G. Panthani, V. Akhavan, B. Goodfellow, J. P. Schmidtke, L. Dunn, A. Dodabalapur, P. F. Barbara and B. A. Korgel, *J. Am. Chem. Soc.*, 2008, **130**, 16770–16777.
54 P. M. Allen and M. G. Bawendi, *J. Am. Chem. Soc.*, 2008, **130**, 9240–9241.

